Journal of Biomedical Optics 8(2), 253–259 (April 2003)

Spatial localization of cardiac optical mapping with multiphoton excitation

Venkat K. Ramshesh
Stephen B. Knisley
The University of North Carolina at Chapel Hill
The Department of Biomedical Engineering
of the School of Medicine
CB #7575, 152 MacNider Hall
Chapel Hill, North Carolina 27599-7575
E-mail: knisley@bme.unc.edu

Abstract. Depth and radius of regions interrogated by cardiac optical mapping with a laser beam depend on photon travel inside the heart. It would be useful to limit the range of depth and radius interrogated. We modeled the effects of a condensing lens to concentrate laser light at a target depth inside the heart, and near infrared excitation to increase penetration and produce two-photon absorption. A Monte Carlo simulation that incorporated a 0.55-NA lens, and absorption and scattering of 1064- or 488-nm laser light in 3-D cardiac tissue indicated the distribution of excitation fluence inside the tissue. A subsequent simulation incorporating absorption and scattering of transmembrane voltage-sensitive fluorescence (wavelength 669 nm) indicated locations from which fluorescence photons exiting the tissue surface originated. The results indicate that mapping at depths up to 300 μm in hearts can provide significant improvement in localization over existing cardiac optical mapping. The estimated interrogation region is sufficiently small to examine cardiac events at a cellular or subcellular scale and may allow mapping at various depths in the heart.
[DOI: 10.1117/1.1559831]

Keywords: heart; transmembrane voltage; Monte Carlo model; near-infrared.

Paper 02026 received Apr. 26, 2002; revised manuscript received Oct. 30, 2002; accepted for publication Nov. 18, 2002.

Introduction

Optical measurements in hearts stained with transmembrane voltage sensitive fluorescent dyes are used to study cardiac action potential propagation, repolarization, arrhythmias, and electric stimulation.[1–4] One of the limitations of conventional optical mapping is that it records events at multiple sites distributed near the tissue surface but cannot record at sites distributed at various depths. Novel methods that employ transillumination or plunge optic fibers have been developed to optically map with limited resolution at various depths, which may allow examination of important arrhythmic behavior throughout ventricular walls.[2,5] Another limitation of optical mapping is the inability to interrogate a microscopic region of tissue. The interrogated region for an individual measurement is in an order of 1 mm due to the scattering of excitation and emission photons in the tissue.[6] As a result, optical mapping has not been able to resolve some potentially important events in hearts, including transmembrane potential changes expected at ends of cells during defibrillation shocks, action potential transmission from a cell to an adjoining cell, and 3-D reentry or microreentry during arrhythmias.[7–9]

In conventional optical mapping with transmembrane voltage sensitive fluorescent dye or green-emitting calcium sensitive fluorescent dye, continuous wave excitation light (typically blue or green wavelengths) is directed onto the heart, while fluorescence light having longer wavelengths that exit the heart surface is collected. The localization for an individual measurement is achieved by either restricting the area of the excitation light with a laser beam while collecting fluorescence from the whole tissue surface (laser scanner method), or by applying the excitation light onto a broad region of the tissue surface while restricting the collection to a small surface area using a camera (broad-field excitation method). It may be possible to achieve 3-D optical mapping and microscopic interrogation by use of long wavelength laser excitation light and a high numerical aperture lens. The long wavelength light undergoes less absorption in the tissue, which may allow deeper interrogation. The lens may concentrate laser excitation light in a small region of the tissue at a given depth, allowing microscopic interrogation at discrete depths. Also, multiphoton excitation, possible with a pulsed near-infrared laser, may reduce interrogated volume by concentration of fluorescence in the focal region due to quadratic dependence of excitation probability on fluence.[10,11] However, due to the high cost of a femtosecond pulsed near-infrared laser, we consider a theoretical model estimate of size and depth of tissue that may be interrogated is beneficial beforehand. To estimate this, we used Monte Carlo computer models that incorporated concentration of laser light with a lens and absorption and scattering of both the laser light and the fluorescence in cardiac tissue.

2 Methods

2.1 Launch of Photons with a Lens

We simulated the use of a convex lens to concentrate the excitation light. Light beams representing a radial section of a conical illumination volume were launched onto the cardiac

1083-3668/2003/$15.00 © 2003 SPIE

tissue at orientations and positions calculated from the diameter, focal length, and distance between the lens and the tissue surface. The number of photons assigned to each beam was increased for beams at greater radii to produce a constant number of photons per tissue surface area illuminated. In simulations presented here, 100 beams were launched in the radial section**.** The lens could be positioned at different distances from the tissue. This allowed alterations in the target depth of the excitation light inside the tissue, i.e., the depth in tissue where the focal point would occur if aberrations, scattering, and absorption of photons were negligible. We chose a lens having a diameter 2.5 cm and focal length 1.9 cm, which represented a lens with numerical aperture of 0.55 in air. This lens has a relatively large numerical aperture for its diameter, and is commercially available. We modeled the lens at distances from the tissue varying from 1.89 to 1.71 cm in steps of 0.01 cm, which produced target depths from 0.01 to a maximum of 0.19 cm below the illuminated tissue surface. To study the excitation light, simulations were performed with optical properties of tissue for light wavelength of 1064 nm, which is similar to wavelengths of spectrally dispersed light that can be produced during femtosecond laser pulses, and 488 nm. We used the measurements performed by Splinter et al. for the absorption coefficient (μ_a =0.3/cm), scattering coefficient (μ_s =177.5/cm), and scattering anisotropy (g =0.964) in cardiac tissue with 1064 nm excitation light.[12] For 488-nm excitation light, we used the measurements performed by Ding et al.[6] for the absorption coefficient (μ_a =5.2/cm), scattering coefficient (μ_s =232.0/cm), and scattering anisotropy (g=0.94). To study the fluorescence propagation, simulations were performed with optical properties of tissue for 669-nm wavelength. We selected 669-nm wavelength to represent the emitted fluorescence because this is near the wavelength of peak fluorescence emitted from the transmembrane voltage-sensitive dye di-4-ANEPPS.[13] Also values of the optical properties of cardiac tissue for this wavelength are available (μ_a =1.0/cm), (μ_s =218.0/cm) and (g=0.96).[6]

2.2 Excitation Light Propagation

We used a Monte Carlo model similar to that developed by Wang et al. to simulate the propagation within the tissue of excitation light from each beam and to determine the excitation light fluence in tissue.[14] The tissue, having a radius of 0.11 cm, and thickness of 0.11 cm was assumed homogenous and cylindrically symmetric. The Monte Carlo model treated the launched photons as classical particles, having no specific phase or polarization. The model used a Cartesian coordinate system in three dimensions for photon propagation. A moving spherical coordinate system, whose *z* axis was dynamically aligned with the photon propagation direction, was used for sampling the change in photon propagation direction due to scattering events. The simulation recorded fluence in each grid element as the summed weights of photons absorbed per unit area of the element normalized to the total weights of the launched photons. The recording of fluence was performed with a homogenous grid system set up in depth and radial coordinates. Since the distribution of recorded fluence was independent of the rotational angle of the radial section of beams, a single section was sufficient to determine the distribution in the radial system. Each simulation launched 270,000 photons distributed among 100 beams, with each beam containing a specific number of photons proportional to the tissue surface area illuminated by the beam. This accounted for the larger area of illuminated tissue surface represented by beams entering tissue at greater distances from the optical axis. The number of photons was chosen because it produced practical computational times and stable results. Stability was verified in additional simulations that showed essentially no changes in results when the number of photons was altered in the range of 200,000 to 500,000. Each photon after entering the tissue underwent a random walk inside the tissue. The step size, i.e., distance traveled in each step, was determined for the photon probabilistically based on the absorption and scattering coefficients. The program then determined whether the photon hit a boundary of the tissue. If it did not hit a boundary, the photon moved to a new location in the tissue based on step size and current propagation direction. At each new location of the photon, part of the photon weight was absorbed and the remaining part scattered. Propagation of the photon continued with a new step size until the weight (w) of the photon fell below a threshold, or it hit a boundary. If weight fell below a threshold the photon with a new weight, calculated as mw, had a probability of $1/m$ to survive and continue propagation. This technique avoided the energy conservation rule violation that would occur if all the photon packets falling below the weight were simply terminated. If a photon hit a boundary, it either reflected back into the tissue or exited from the tissue, depending on its current direction and refractive index of the tissue. When all the photons were launched and their absorption was recorded, the fluence rate distribution inside the tissue approached realistic values. Preliminary simulations with a grid size of 11 μm indicated that interrogated regions might be smaller than 11 μm. All results presented here used a grid with element size 1.1 μm. This value is comparable to the wavelength of the near-infrared excitation light. Each simulation to determine the distribution of fluence in radial and depth coordinates required 2.4 min of computation time on an Intel Pentium processor (933 MHz) for the 1064-nm excitation and 1.5 min for the 488-nm excitation. Output file size was 38 megabytes.

2.3 Fluorescence Light Propagation

Each grid element was regarded as a fluorescence point source. The weight of the fluorescence photon launched from each grid element was proportional to either the fluence of the excitation light for that element or the square of this fluence, representing either single or two-photon excitation.[10] The initial direction of photon propagation was assumed isotropic. Thus, locations of origin, weights, and directions of all fluorescence photons were specified. During this simulation, weights of all fluorescence photons that exited the top surface of the tissue and the locations of their origin in the tissue were recorded. From these, we determined the total weights of all fluorescence photons that exited, which can be considered proportional to the signal collected with a large area collector such as a photomultiplier tube. Using the recorded locations, we determined the specific region inside the tissue from which a given percentage of the total exiting fluorescence originated.

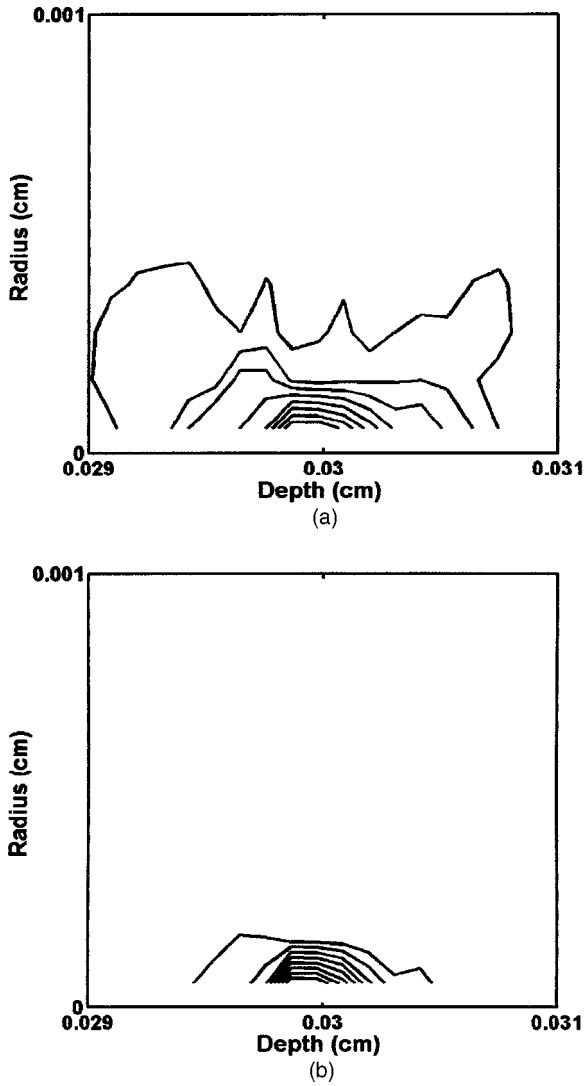

Fig. 1 Results of Monte Carlo simulation showing distributions of the fluence (a) and the square of the fluence (b) of excitation light as functions of radius and depth in tissue. The fluence in tissue was modeled with absorption and scattering properties of light having wavelength 1064 nm. The distance of the lens from the tissue surface was 1.87 cm, which produced a target depth 0.03 cm inside the tissue. (a) The innermost contour represents grid elements in which the fluence was 0.9 of its maximum. Contours decrease with distance from the maximum with step size 0.1. The outermost contour represents elements where the fluence was 0.2 of its maximum. (b) The innermost contour represents elements in which the square of the fluence was 0.9 of its maximum. Contours decrease with distance from the maximum with step size 0.1. The outermost contour represents grid elements where the square of fluence was 0.2 of its maximum.

3 Results

3.1 Fluence of Excitation Light in Tissue

Figure 1(a) shows the distribution of fluence of 1064-nm laser excitation light in the modeled region near the location of greatest fluence. The fluence at a given location is proportional to the probability of single-photon absorption. The distance between the lens and tissue was adjusted to produce a target depth in the tissue of 300 μm. Each contour indicates the depths and radii inside the tissue at which fluence had a constant value. The grid element of maximum fluence had a depth 299 μm and radius 0.55 μm, which is the radius representing elements nearest the optical axis. Fluence decreased at larger radii and at depths greater than or less than the depth of maximum fluence. The outermost contour indicates fluence decreased to 0.2 of its maximum value at depths having a maximum range approximately 10 μm greater or less than the target depth and at radii having a maximum of 4 μm. When optical properties for 488-nm excitation light were used instead of those for 1064-nm light, the grid element of maximum fluence had a depth of 298.5 μm and radius 0.55 μm (not shown). The fluence decreased to 0.2 of its maximum value at depths 7.5μm greater or less than the target depth and at radii having a maximum of 7.5 μm. Local maxima were also observed at sites away from the target depth for both wavelengths.

Figure 1(b) shows the distribution of the square of the fluence of the excitation light in the same model used for Fig. 1(a). The square of fluence is proportional to probability of two-photon absorption. The outermost contour indicates the square of fluence decreased to 0.2 of its maximum value at depths having a maximum range of 6 μm greater or less than the target depth and at radii having a maximum of 1.7 μm. When the optical properties for 488-nm excitation light were used, the square of fluence decreased to 0.2 of its maximum value at depths having a maximum range of 5 μm greater or less than the target depth and at radii having a maximum of 1.5 μm. This indicates the region of excitation for the 488-nm light was similar or slightly smaller than it was for 1064-nm light. Also, for both excitation wavelengths, two-photon excitation was much more concentrated in both depth and radial directions compared with single photon excitation.

These results indicate a region of high excitation light fluence occurs at a certain depth in heart tissue. The depth may be limited by absorption and scattering of the excitation light. These may cause light to become more diffuse at a greater depth. To test this, distance between the lens and tissue was varied to produce different target depths. For each target depth, we determined the maximum and minimum depths and the maximum radius inside the tissue (Dmax, Dmin, Rmax) at which excitation light fluence was greater than 0.5 of the maximum value of the fluence. We chose the 0.5 level of fluence in the summary of Dmax, Dmin, and Rmax, because at a given depth higher fluence increases the chance to produce fluorescence photons that exit the tissue. We also determined the Dmax, Dmin, and Rmax, at which the square of the excitation light fluence was greater than 0.5 of its maximum.

Figure 2 shows a summary of the results from four simulations with 1064-nm excitation light in which target depths ranged from 100 to 400 μm in the tissue in steps of 100 μm. The range of depth of concentrated excitation fluence determined for all grid elements in the model is indicated by the range from Dmax (filled diamonds) to Dmin (open squares). The maximum radius is indicated by Rmax (filled circles). For a given target depth of 100 to 300 μm, Dmax and Dmin were almost the same. Their difference was $\leqslant$ 10 μm for the fluence [Fig. 2(a)] and $\leqslant$ 4 μm for the square of fluence [Fig. 2(b)], indicating that excitation light was localized axially (i.e., in the depth direction on the optical axis) in a region near the target depth. When the target depth was increased to 400

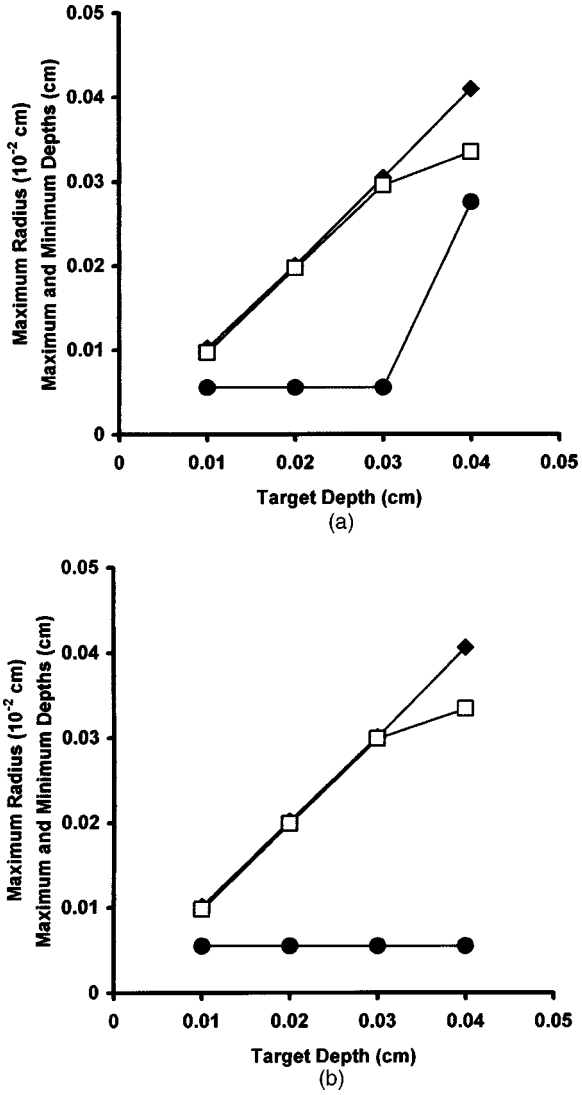

Fig. 2 Results of Monte Carlo simulations showing the maximum and minimum depths and maximum radii inside the tissue where (a) excitation light fluence or (b) the square of fluence was greater than 0.5 of its respective maximum value. The filled diamonds and the open squares indicate the maximum and minimum depths, respectively. The filled circles indicate the maximum radii. The depths and radii are plotted versus the target depth. Note that the ordinate scale for radii is 100 times smaller than the scale for the depths. The light propagation in tissue was based on absorption and scattering properties of light having wavelength 1064 nm.

μm, the difference between Dmax and Dmin increased to 75 μm for the fluence and 72 μm for the square of fluence, indicating that the excitation light became markedly diffuse for the 400 μm target depth compared with that for the smaller target depths. For the fluence, Rmax was $\leqslant$ 0.55 μm when the target depth was 100 to 300 μm, while it was 2.75 μm when the target depth was 400 μm. For the square of the fluence, Rmax was $\leqslant$ 0.55 μm for all target depths. These results indicate that excitation light was concentrated radially.

When optical properties for 488-nm excitation light were used, differences between Dmax and Dmin for target depths $\leqslant$ 200 μm were 5 μm for fluence and 2 to 4 μm for the square of fluence. The differences for target depths of 300 to 400 μm increased markedly reaching 115 to 307 μm for fluence and 50 to 230 μm for the square of fluence. This indicates effects of light diffusion became marked at an approximately 100 μm shallower depth for the 488-nm light compared with the results for 1064-nm excitation described before. The Rmax for the fluence was $\leqslant$ 0.55 μm at target depths of 100 to 300 μm, and became 1.65 μm at a target depth of 400 μm. For target depths of 100 to 400 μm, Rmax was $\leqslant$ 0.55 μm for the square of the fluence.

Thus for both excitation light wavelengths studied, the small Rmax indicates excitation was radially concentrated close to the optical axis for target depths to 400 μm. However, the difference between Dmax and Dmin was larger than Rmax and became greater as the target depth was increased (Fig. 2). This indicates loss of concentration in the axial direction was a more important limitation than radial loss of concentration. In our subsequent analysis of spatial localization of fluorescence, we used a target depth of 300 μm because this was the approximate maximum depth at which further increase in depth caused a very marked loss of concentration in the axial direction. Localization at this target depth represented a worst-case estimate for target depths less than 300 μm.

3.2 Dimensions of Tissue Interrogated

In hearts stained with transmembrane voltage-sensitive fluorescent dye, excitation photons can be absorbed by fluorescent dye molecules, thus producing fluorescence photons. The production of the fluorescence photons was simulated by launching new photons at grid elements in the tissue. Initial weights of the photons were proportional to the fluence or square of fluence in each grid element. The propagation of the photons in the tissue was then modeled with the Monte Carlo method. For the fluorescence propagation, we used the absorption and scattering coefficients of light having wavelength 669 nm that were measured in heart tissue.[6]

Results are shown in Fig. 3 for a target depth of 300 μm and 1064-nm excitation light. Figure 3(a) shows the results obtained when original weights of fluorescence photons were proportional to excitation fluence. Figure 3(b) shows results when original weights of fluorescence photons were proportional to the square of excitation fluence. Comparison of Fig. 3(a) with Fig. 3(b) indicates that for a given percentage, the radii and range of depth were smaller when the original weights were proportional to the square of the excitation fluence.

Results for excitation light wavelength 488 nm are shown in Fig. 4. The major difference compared with Fig. 3 is a leftward movement of the contour for a given percentage, indicating the region of origin of the exiting fluorescence was closer to the tissue surface. Also, the maximum radius of contours became larger for the 488-nm excitation compared with 1064-nm excitation.

4 Discussion

This modeling study was performed to estimate spatial localization of optical mapping with two-photon excitation in hearts. We sought to quantify the extent to which two-photon excitation can overcome two limitations of conventional optical mapping. One of the limitations is the inability to record

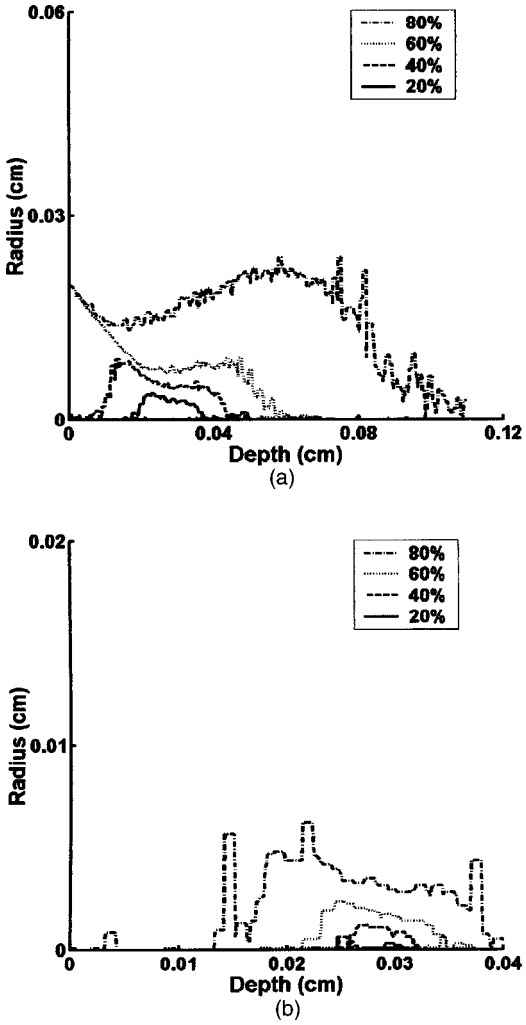

Fig. 3 Results of Monte Carlo simulations showing dimensions in radius and depth of the tissue within which a given percentage of the exiting fluorescence originated and for which the exiting photons had the greatest weights. The excitation wavelength was 1064 nm. The fluorescence propagation in tissue was based on absorption and scattering properties of light having wavelength 669 nm. Results are shown for percentages 20, 40, 60, and 80. The target depth was 0.03 cm. (a) shows the results when the original weights of fluorescence photons were proportional to the fluence of the excitation light. (b) shows the results when the original weights of fluorescence photons were proportional to the square of the fluence of the excitation light. Note the smaller scale in (b).

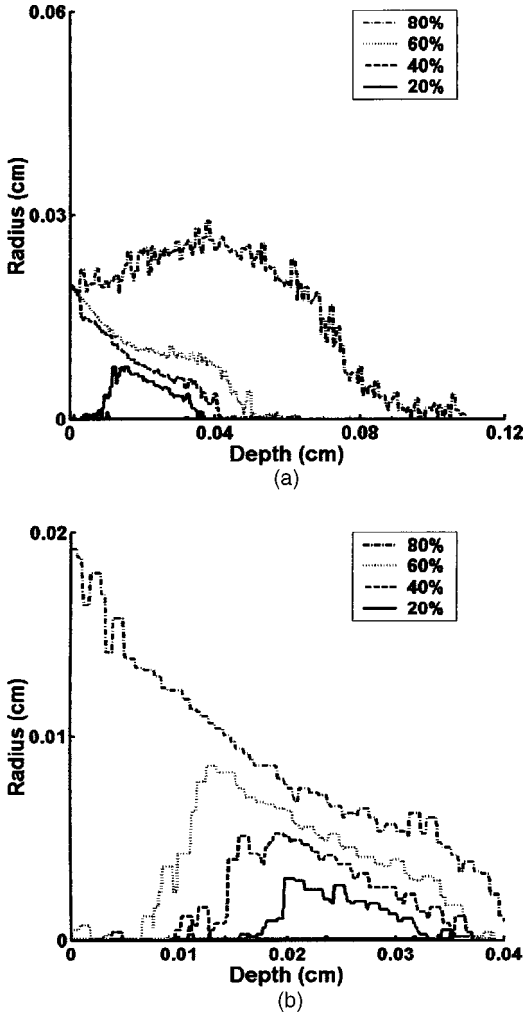

Fig. 4 Results of Monte Carlo simulations showing dimensions in radius and depth of the tissue within which a given percentage of the exiting fluorescence originated and for which the exiting photons had the greatest weights. The excitation wavelength was 488 nm. The fluorescence propagation in tissue was based on absorption and scattering properties of light having wavelength 669 nm. Percentages shown and target depth were the same as those in Fig. 3. (a) shows the results when the original weights of fluorescence photons were proportional to the fluence of the excitation light. (b) shows the results when the original weights of fluorescence photons were proportional to the square of the fluence of the excitation light. Note the smaller scale in (b).

at various depths in the heart. Another limitation is the inability to interrogate a region of tissue having a size comparable to the size of cardiac cells. With multiphoton excitation, a longer wavelength of excitation light is used, which may allow light penetration to a greater depth compared with the penetration for shorter wavelengths. A condensing lens can direct the excitation light toward a region below the heart surface, which may allow signals from a specific depth in the heart to be distinguished. Also, with two-photon excitation, the probability of excitation is proportional to the square of the excitation fluence. Excitation may then be concentrated near a local maximum, which may reduce the size of heart tissue interrogated at each recording site.

We used a Monte Carlo model of excitation light transport in three-dimensional cardiac tissue to estimate fluence (i.e., excitation) in the heart for 1064- or 488-nm light. We launched the excitation photons at angles and locations on the tissue surface to simulate light directed with a condensing lens toward a point at a given depth inside the tissue. We then used the distribution of excitation fluence determined from this model in another Monte Carlo model to estimate the size and location of the region of origin of fluorescence photons that exited the tissue surface. In each simulation, we used values of the absorption, scattering, and scattering anisotropy coefficients that have been measured in heart tissue.[6,12]

4.1 Interrogated Region

One finding is that the interrogated region spanned a range of depth that was consistently greater than its width (Figs. 3 and 4). Figure 3(b) shows with 1064-nm excitation light and two-photon excitation at a target depth of 300 μm, 80% of the exiting fluorescence originates in tissue having a range of depth approximately 4 to 5 times its radius. Therefore, the radial spread alone does not adequately describe localization for two-photon fluorescence mapping in hearts.[15] Also, a single value for the radial spread is not sufficient to fully describe the interrogated region, because the end of the interrogated region nearer the tissue surface is wider than the deep end (Figs. 3 and 4).

The main finding is that interrogated regions for two-photon excitation in hearts are smaller than those reported for conventional cardiac optical mapping. In conventional laser scanning with a laser beam radius of 0.1 mm, the reported depth of the region from which 80% of the fluorescence originated spanned 0 to 750 μm and the maximum radius of the region was 240 μm [Fig. 6(a) of Ref. 6]. Here, we find that the two-photon interrogation region for a target depth of 300 μm is approximately 1/3 as large as those reported. The interrogation region at shallower depths is even smaller due to the decreased range of depth of the excited region (Fig. 2).

The model does not incorporate all factors that affect the light transport and excitation. Broadening of the pulse width as excitation light travels in the heart may lessen peak fluence and two-photon excitation.[16,17] Also aberrations due to mismatch of the refractive index in different media affect light transport.[18] Our additional simulations (unpublished) indicate for a given target depth, the region of interrogation extends somewhat deeper when effects of refractive index mismatch are included in the calculation. A correction method that compensated for effects of the mismatch has been described.[19] Also, effects of aberration may be reduced for two-photon excitation.[20]

When single photon excitation is considered, the size of the interrogated region for a target depth of 300 μm is comparable to that for conventional cardiac mapping found by Ding et al.[6] [e.g., range of depth and radius are approximately 0 to 1100 μm and 250 μm for 1064 nm excitation in Fig. 3(a) and 0 to 800 μm and 275 μm for 488-nm excitation in Fig. 4(a)]. The finding that the brightest exiting fluorescence originated in regions below the surface [e.g., 20% contours in Figs. 3(a) and 4(a)] indicates that a condensing lens may help in distinguishing signals from regions below the heart surface even with single photon excitation.

An interesting finding of this study is the variation in maximum radii of contours of fluence and the square of fluence. The 0.2 contours of fluence for all target depths studied had larger maximum radii for 488-nm light compared to 1064-nm light. However, when 0.5 contours of fluence are considered, the maximum radius for the 400-μm target depth was smaller for the 488-nm light (1.65 μm for 488 nm versus 2.75 μm for 1064 nm). Also, for the square of fluence, maximum radius of the 0.2 contour found for the target depth of 300 μm was slightly smaller with the 488-nm light (1.5 μm) compared with 1064-nm light (1.7 μm). Radii may be influenced by effects of multiple factors that differ for the two wavelengths, including tissue absorption, scattering, and anisotropy that influence the distribution of fluence. For example, the smaller absorption coefficient for 1064-nm light may allow scattered photons to reach a greater radius before they are absorbed, while the greater scattering coefficient for the 488-nm light may cause photons to travel away from the target, which would also increase the radius.

The wavelength of excitation light influences the depth of the interrogated region. Comparison of Figs. 3 and 4 indicate that regions from which a given percentage of the exiting fluorescence originated are closer to the tissue surface when the excitation light wavelength is 488 versus 1064 nm. This may occur because the light having shorter wavelength undergoes greater absorption in the tissue, decreasing the fluorescence excitation at deeper sites in the tissue.

4.2 Implications for Optical Mapping of the Heart

The spatial localization of cardiac optical mapping has not been sufficient to resolve transmembrane voltages at ends of individual cells (typical cell size 20 $\times$ 100 μm) or unit bundles containing many tightly coupled cells in cardiac tissue or hearts. Cardiac electrophysiological models have predicted these transmembrane voltages alter during an electrical stimulation pulse, which may be a mechanism for the electrical induction of arrhythmias and electrical defibrillation of the heart.[21,22] Methods to measure transmembrane voltages at ends of isolated cells have required localization on the order of 5 μm.[23–25]

Improved localization of optical mapping may be used to examine action potential propagation from cell to cell in the heart. This has only been examined in isolated cultured cell strands or monolayers.[26] Also, improved localization may allow tests of whether microreentrant circuits can occur and whether they produce arrhythmias in the heart.[9]

The range of depth of localization in our analysis suggests optical mapping may be performed in 3-D without transillumination or optical fibers inserted into the tissue.[2,5] Figure 2 indicated changes in the interrogation depth may be accomplished by altering the distance between the lens and tissue. However, mapping at target depths greater than 300 to 400 μm will increase the range of depths within which the excitation light has relatively high fluence, ultimately increasing the size of the interrogated region. At depths up to 300 μm, the region inside the tissue where the fluence is 0.5 of its maximum [$\leqslant$ 4 μm, Fig. 2(b)] is smaller than a cardiac cell, suggesting that it is possible to test the predictions of changes in transmembrane voltage on a subcellular spatial scale during shocks.

A relatively large signal level is important for cardiac optical mapping with the laser scanner method. Since the dwell time of the laser beam at a given spot during laser scanning can be under 10 μs, there is little time for integration or temporal averaging of light during a sample. To obtain a smooth recording of the action potential, the collected fluorescence must be sufficiently intense so that it is not dominated by discrete pulses produced by individual fluorescence photons. The optical mapping described here, in which fluorescence photons exit the tissue and can be collected regardless of whether or not they scatter, may avoid loss of signal intensity that occurs when a confocal pinhole is used. This loss can be very large, e.g., in the simulation of Fig. 3(a), the

total weight of exiting photons that did not scatter was only 0.15 % of the total weight of all exiting photons.

5 Conclusion

Existing cardiac optical mapping has used blue or green excitation light. This study has evaluated an alternative that may use near-infrared excitation light. Cardiac optical mapping with a condensing lens and near-infrared light for two-photon excitation at depths up to 300 μm in hearts may provide significant improvement in localization over existing cardiac optical mapping. The estimated interrogation region is sufficiently small to examine cardiac events at a cellular or subcellular scale. The mapping may be performed at various depths in the heart by altering the distance between the tissue and the lens.

Acknowledgments

Supported by National Institutes of Health Grants HL52003, HL67728, and American Heart Association Grant 9740173N. S.B.K. is an Established Investigator Awardee of the American Heart Association.

References

1. I. R. Efimov, D. T. Huang, J. M. Rendt, and G. Salama, ''Optical mapping of repolarization and refractoriness from intact hearts,'' *Circ. Res.* **90**(3), 1469–1480 (1994).
2. W. T. Baxter, S. F. Mironov, A. V. Zaitsev, J. Jalife, and A. M. Pertsov, ''Visualizing excitation waves inside cardiac muscle using transillumination,'' *Biophys. J.* **80**(1), 516–530 (2001).
3. S. B. Knisley, ''Transmembrane voltage changes during unipolar stimulation of rabbit ventricle,'' *Circ. Res.* **77**(6), 1229–1239 (1995).
4. D. S. Rosenbaum, ''Optical mapping of cardiac excitation and arrhythmias: A primer,'' *Optical Mapping of Cardiac Excitation and Arrhythmias*, D. Rosenbaum and J. Jalife, Eds., pp. 2–7, Futura Publishing Company, Armonk, NY (2001).
5. D. A. Hooks, I. J. LeGrice, J. D. Harvey, and B. H. Smaill, ''Intramural multisite recording of transmembrane potential in the heart,'' *Biophys. J.* **81**(5), 2671–2680 (2001).
6. L. Ding, R. Splinter, and S. B. Knisley, ''Quantifying spatial localization of optical mapping with monte carlo simulations,'' *IEEE Trans. Biomed. Eng.* **48**(10), 1098–1107 (2001).
7. R. Plonsey and R. C. Barr, ''Electric field stimulation of excitable tissue,'' *IEEE Trans. Biomed. Eng.* **42**(4), 329–336 (1995).
8. S. Rohr, J. P. Kucera, and A. G. Kléber, ''Slow conduction in cardiac tissue, I: Effects of a reduction of excitability versus a reduction of electrical coupling on microconduction,'' *Circ. Res.* **83**(8), 781–794 (1998).
9. M. S. Spach and P. C. Dolber, ''Relating extracellular potentials and their derivatives to anisotropic propagation at a microscopic level in human cardiac muscle. Evidence for electrical uncoupling of side-to-side fiber connections with increasing age,'' *Circ. Res.* **58**(3), 356–371 (1986).
10. A. Fischer, C. Cremer, and E. H. K. Stelzer, ''Fluorescence of coumarins and xanthenes after two-photon absorption with a pulsed titanium-sapphire laser,'' *Appl. Opt.* **34**(12), 1989–2003 (1995).
11. X. Gan and M. Gu, ''Spatial distribution of single-photon and two-photon fluorescence light in scattering media: Monte Carlo simulation,'' *Appl. Opt.* **39**(10), 1575–1579 (2000).
12. R. Splinter, R. H. Svenson, L. Littmann, J. R. Tuntelder, C. H. Chuang, G. P. Tatsis, and M. Thompson, ''Optical properties of normal, diseased, and laser photocoagulated myocardium at the Nd:YAG wavelength,'' *Lasers Surg. Med.* **11**(2), 117–124 (1991).
13. E. Fluhler, V. G. Burnham, and L. M. Loew, ''Spectra membrane binding, and potentiometric responses of new charge shift probes,'' *Biochemistry* **24**, 5749–5755 (1985).
14. L. Wang, S. L. Jacques, and L. Zheng, ''MCML—Monte Carlo modeling of light transport in multi-layered tissues,'' *Comput. Methods Programs Biomed.* **47**(2), 131–146 (1995).
15. A. K. Dunn, V. P. Wallace, M. Coleno, M. W. Berns, and B. J. Tromberg, ''Influence of optical properties on two-photon fluorescence imaging in turbid samples,'' *Appl. Opt.* **39**(7), 1194–1201 (2000).
16. V. R. Daria, C. Saloma, and S. Kawata, ''Excitation with a focused, pulsed optical beam in scattering media: diffraction effects,'' *Appl. Opt.* **39**(28), 5244–5255 (2000).
17. C. M. Blanca and C. Saloma, ''Efficient analysis of temporal broadening of a pulsed focused Gaussian beam in scattering media,'' *Appl. Opt.* **38**(25), 5433–5437 (1999).
18. M. J. Booth and T. Wilson, ''Refractive-index-mismatch induced aberrations in single-photon and two-photon microscopy and the use of aberration correction,'' *J. Biomed. Opt.* **6**(3), 266–272 (2001).
19. M. A. A. Neil, R. Justkaitis, M. J. Booth, T. Wilson, T. Tanaka, and S. Kawata, ''Adaptive aberration correction in a two-photon microscope,'' *J. Microsc.* **200**, 105–108 (2000).
20. D. Ganic, X. Gan, and M. Gu, ''Reduced effects of spherical aberration on penetration depth under two-photon excitation,'' *Appl. Opt.* **39**(22), 3945–3947 (2000).
21. S. B. Knisley, W. M. Smith, and R. E. Ideker, ''Effect of field stimulation on cellular repolarization in rabbit myocardium: Implications for reentry induction,'' *Circ. Res.* **70**(4), 707–715 (1992).
22. W. Krassowska, T. C. Pilkington, and R. E. Ideker, ''Potential distribution in three-dimensional periodic myocardium. Part I. Solution with two-scale asymptotic analysis,'' *IEEE Trans. Biomed. Eng.* **37**(3), 252–266 (1990).
23. S. B. Knisley, T. F. Blitchington, B. C. Hill, A. O. Grant, W. M. Smith, T. C. Pilkington, and R. E. Ideker, ''Optical measurements of transmembrane potential changes during electric field stimulation of ventricular cells,'' *Circ. Res.* **72**(2), 255–270 (1993).
24. H. Windisch, H. Ahammer, P. Schaffer, W. Müller, and D. Platzer, ''Fast optical potential mapping in single cardiomyocytes during field stimulation,'' *Proc. 14th Ann. Intl. Conf. IEEE Eng. Med. Biol. Soc.* **14**, 634–635 (1992).
25. D. K.-L. Cheng, L. Tung, and E. A. Sobie, ''Nonuniform responses of transmembrane potential during electric field stimulation of single cardiac cells,'' *Am. J. Physiol.* **277**(1), H351–H362 (1999).
26. V. G. Fast and A. G. Kléber, ''Microscopic conduction in cultured strands of neonatal rat heart cells measured with voltage-sensitive dyes,'' *Circ. Res.* **73**(5), 914–925 (1993).